

# Paraxial Theory of Direct Electro-Optic Sampling of the Quantum Vacuum

A.S. Moskalenko,\* C. Riek, D.V. Seletskiy, G. Burkard, and A. Leitenstorfer  
*Department of Physics and Center for Applied Photonics,  
 University of Konstanz, D-78457 Konstanz, Germany*  
 (Dated: April 3, 2018)

Direct detection of vacuum fluctuations and analysis of sub-cycle quantum properties of the electric field are explored by a paraxial quantum theory of ultrafast electro-optic sampling. The feasibility of such experiments is demonstrated by realistic calculations adopting a thin ZnTe electro-optic crystal and stable few-femtosecond laser pulses. We show that nonlinear mixing of a short near-infrared probe pulse with multi-terahertz vacuum field modes leads to an increase of the signal variance with respect to the shot noise level. The vacuum contribution increases significantly for appropriate length of the nonlinear crystal, short probe pulse durations, tight focusing, and sufficiently large number of photons per probe pulse. If the vacuum input is squeezed, the signal variance depends on the probe delay. Temporal positions with noise level below the pure vacuum may be traced with a sub-cycle accuracy.

PACS numbers: 42.50.Ct, 42.50.Lc, 42.65.Re, 78.20.Jq

Finite fluctuation amplitudes in the ground state of empty space represent the ultimate hallmark of the quantum nature of the electromagnetic radiation field. These vacuum fluctuations manifest themselves indirectly in a number of phenomena that are accessible to spectroscopy such as the spontaneous decay of excited atomic states as well as the Lamb shift [1] in atoms [2] and in quantum-mechanical electric circuits [3]. Access to the quantum aspects of electromagnetic radiation is provided by the analysis of photon correlation [4, 5] or homodyning [6–11] measurements. However, these approaches require amplification of the quantum field under study to finite intensity and averaging of the information over multiple optical cycles.

On the other side, precise determination of voltage or electric field amplitude as a function of time represents a fundamental task in science and engineering. Optical techniques have to be applied when detecting electric fields oscillating in the terahertz (THz) range and above. Those approaches involve probing with ultrashort laser pulses of a temporal duration on the order of half an oscillation period at the highest frequencies under study. Far-infrared electric transients [12, 13] can be characterized by photoconductive switching [14]. Electro-optic sampling in free space [15–17] allows field-resolved detection at high sensitivity in the entire far- and mid-infrared spectral range [18, 19]. Direct studies of the complex-valued susceptibilities of materials and the elementary dynamics in condensed matter may be performed with these methods [20, 21]. The time integral of near-infrared to visible electric-field wave packets is accessible with attosecond streaking [22]. So far, all those techniques were restricted to the classical field amplitude.

In this Letter, we demonstrate theoretically that the quantum properties of light may be accessed directly in the time domain, i.e. with sub-cycle temporal resolution. Our considerations are based on the realistic example of electro-optic detection with zincblende-type materials

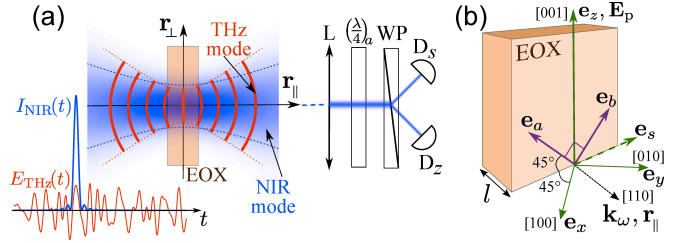


FIG. 1. (color online) Electro-optic sampling setup and geometry. (a) The incoming near-infrared (NIR) probe and multi-THz signal fields mix in the electro-optic crystal (EOX). The NIR (blue) spatial mode amplitude is depicted by the contour plot whereas a sampled THz (red) spatial mode is indicated by wave fronts. Bottom left corner: time profiles of the NIR intensity envelope  $I_{\text{NIR}}(t)$  and a representative multi-THz vacuum field  $E_{\text{THz}}(t)$ . After collimation by a lens (L), the modified NIR field is analyzed using a quarter-wave plate ( $\frac{\lambda}{4}$ ), a Wollaston prism (WP) and balanced detectors ( $D_s, D_z$ ) measuring the difference in the photon flux for the split components. (b) Spatial directions determining the electro-optic effect in the zincblende-type EOX and the following ellipsometry analysis.

[23]. Even vacuum fluctuations may be sampled without amplification by broadband probing of electric field amplitudes in the multi-THz region with few-femtosecond laser pulses of moderate energy content.

We consider the geometry of electro-optic sampling shown in Fig. 1. An ultrashort near-infrared (NIR) wave packet with electric field  $\mathbf{E}_p$  propagates along the [110] axis of an electro-optic crystal (EOX) [23, 24]. Its wave vector  $\mathbf{k}_\omega$  is perpendicular to the  $z$ -axis  $\mathbf{e}_z$  of the EOX. We select  $\mathbf{E}_p \parallel \mathbf{e}_z$  [25]. In this configuration, the second-order nonlinear mixing of  $\mathbf{E}_p(t)$  with an incident THz field  $\hat{\mathbf{E}}_{\text{THz}}(t)$  induces nonlinear polarization in the EOX plane with the components (for details, see Ref. [25])

$$\hat{P}_s^{(2)}(t) = -\epsilon_0 d \hat{E}_{\text{THz},s}(t) E_p(t), \quad \hat{P}_z^{(2)}(t) = 0. \quad (1)$$

$\epsilon_0$  is the vacuum permittivity. The coupling constant  $d = -n^4 r_{41}$  can be determined from the electro-optic coefficient  $r_{41}$  and refractive index (RI)  $n$  at the central frequency  $\omega_c$  of  $\mathbf{E}_p$  [26–28]. In general, both fields  $\hat{E}_{\text{THz}} \equiv \hat{E}_{\text{THz},s}$  and  $\hat{P}_s^{(2)}$  in Eq. (1) are quantized, whereas  $E_p = E_{p,z} = \langle \hat{E}_{p,z} \rangle$  denotes the classical part of the probe field. We neglect the effect of quantum mechanical fluctuations of the probe field on  $\hat{\mathbf{P}}^{(2)}$ , assuming a sufficiently large  $E_p$ .

The nonlinear polarization  $\hat{\mathbf{P}}^{(2)}$  generated by the wave mixing in the EOX represents a source in the inhomogeneous wave equation describing propagation of the electric field  $\hat{\mathbf{E}}$  in the EOX. The fields  $\hat{\mathbf{F}} = \hat{\mathbf{E}}, \hat{\mathbf{P}}^{(2)}$  propagating in the forward direction  $r_{\parallel}$  (see Fig. 1) can be decomposed as  $\hat{\mathbf{F}}(\mathbf{r}, t) = \int_{-\infty}^{\infty} d\omega \hat{\mathbf{F}}(\mathbf{r}; \omega) e^{i(k_{\omega} r_{\parallel} - \omega t)}$ , where  $k_{\omega} = \omega n_{\omega}/c_0$ .  $c_0$  and  $n_{\omega}$  are the velocity of light and the frequency-dependent RI of the EOX, respectively. Using the paraxial approximation [29, 30], the inhomogeneous wave equation reads

$$\left[ \Delta_{\perp} + 2ik_{\omega} \frac{\partial}{\partial r_{\parallel}} \right] \hat{\mathbf{E}}(\mathbf{r}; \omega) = -\frac{\omega^2}{\epsilon_0 c_0^2} \hat{\mathbf{P}}^{(2)}(\mathbf{r}; \omega), \quad (2)$$

where  $\mathbf{r}_{\perp} = (r_s, r_z)$  and  $\Delta_{\perp} = \frac{\partial^2}{\partial r_s^2} + \frac{\partial^2}{\partial r_z^2}$ . From Eq. (1) we obtain  $\hat{P}_s^{(2)}(\mathbf{r}; \omega) = -\epsilon_0 d \int_{-\infty}^{\infty} d\Omega \hat{E}_{\text{THz}}(\mathbf{r}; \Omega) E_p(\mathbf{r}; \omega - \Omega) e^{i(k_{\Omega} + k_{\omega - \Omega} - k_{\omega}) r_{\parallel}}$ . The electric field of the probe beam provides a solution of the homogeneous part of Eq. (2) which can be decomposed into Laguerre-Gaussian (LG) modes [31, 32] (see Ref. [25]). We adopt a probe pulse train with a fundamental Gaussian transverse mode of amplitude  $\alpha_p(\omega)$ :

$$E_p(\mathbf{r}; \omega) = \alpha_p(\omega) \text{LG}_{00}(\mathbf{r}_{\perp}, r_{\parallel}; k_{\omega}). \quad (3)$$

A length  $l$  of the EOX much shorter than the Rayleigh range of a beam at the relevant THz frequencies  $\Omega$  with waist size  $w_0$  is assumed, i.e.  $l \ll k_{\Omega} w_0^2/2$ .

The EOX is located at the beam waist,  $r_{\parallel} = 0$ , and has anti-reflection coating on its surfaces. Denoting  $\hat{\mathbf{F}}(\mathbf{r}_{\perp}; \omega) \equiv \hat{\mathbf{F}}(\mathbf{r}_{\perp}, r_{\parallel} = 0; \omega)$  we find that at the exit from the EOX,  $r_{\parallel} = l/2$ , the total electric field in the (110) plane is given by

$$\hat{\mathbf{E}}'(\mathcal{Y}) = E_p(\mathcal{Y}) \mathbf{e}_z + \hat{E}^{(2)}(\mathcal{Y}) \mathbf{e}_s + \delta \hat{\mathbf{E}}'(\mathcal{Y}), \quad (4)$$

where  $\mathcal{Y} \equiv \{\mathbf{r}_{\perp}; \omega\}$ .  $\delta \hat{\mathbf{E}}'(\mathcal{Y}) = \hat{\mathbf{E}}_p(\mathcal{Y}) - E_p(\mathcal{Y}) \mathbf{e}_z$  denotes the vacuum field contribution at the probe frequency  $\omega$  in the vacuum picture [33]. The correction to the probe field generated in the EOX is evaluated as

$$\hat{E}^{(2)}(\mathbf{r}_{\perp}; \omega) = \int_{-\infty}^{\infty} d\Omega \hat{E}_{\text{THz}}(\mathbf{r}_{\perp}; \Omega) E_p(\mathbf{r}_{\perp}; \omega - \Omega) \zeta_{\omega, \Omega}, \quad (5)$$

where the factor  $\zeta_{\omega, \Omega} = -id \frac{l\omega}{2c_0 n} \text{sinc} \left[ \frac{l\Omega}{2c_0} (n_{\Omega} - n_g) \right]$  determines phase matching. Here  $\text{sinc}(x) \equiv \sin(x)/x$ ,  $n_{\Omega}$

is the RI at  $\Omega$ , whereas  $n$  and  $n_g$  are the RI and the group RI  $c_0 \partial k_{\omega} / \partial \omega$  at  $\omega = \omega_c$ , respectively. Going beyond Ref. 17 where an expression similar to Eq. (5) was derived for the case of plane waves in order to establish a classical theory of electro-optic sampling, Eqs. (4) and (5) include the transverse spatial dependence of the fields, the quantized form of the signal as well as the contribution of quantum fluctuations at the probe frequencies. These points are crucial for our further analysis.

From Eq. (4), we see that the nonlinear mixing of the probe and THz components generates a new field propagating in the same direction and polarized perpendicular to the probe. For the analysis of the polarization state of the modified probe, we consider the field components in the coordinate frame  $\mathbf{e}_a = (\mathbf{e}_z \mp \mathbf{e}_s)/\sqrt{2}$  rotated by  $45^\circ$  with respect to the  $\mathbf{e}_{z,s}$  frame [Fig. 1(b)],  $\hat{E}'_a(\mathcal{Y}) = E_p(\mathcal{Y}) [1 \pm i\hat{\phi}(\mathcal{Y})]/\sqrt{2} + \delta \hat{E}'_a(\mathcal{Y})$ . Here  $\hat{\phi}(\mathcal{Y}) = i\hat{E}^{(2)}(\mathcal{Y})/E_p(\mathcal{Y})$  must be small for the frequency range of the probe.

The ellipsometry setup used in typical experiments is explained in Fig. 1(a). We consider its effects at the exit surface of the EOX. This simplification is justified when all probe photons are detected without spatial filtering. The first step of the analysis consists in describing the action of the quarter-wave plate with axes oriented along  $\mathbf{e}_a$  and  $\mathbf{e}_b$  such that it phase-shifts the  $a$ -component of the field by  $\pi/2$ :  $\hat{E}''_a(\mathcal{Y}) = i\hat{E}'_a(\mathcal{Y})$ ,  $\hat{E}''_b(\mathcal{Y}) = \hat{E}'_b(\mathcal{Y})$ . The Wollaston prism splits the electric field into its  $z$ - and  $s$ -components:

$$\hat{E}''_s(\mathcal{Y}) = \frac{e^{\pm i\frac{\pi}{4}} E_p(\mathcal{Y})}{\sqrt{2}} [1 \mp \hat{\phi}(\mathcal{Y})] + \delta \hat{E}''_s(\mathcal{Y}). \quad (6)$$

Finally, the photon numbers in both field components are detected and subtracted. The photon number operator for the polarization  $\alpha = z, s$  reads [34]

$$\hat{\mathcal{N}}_{\alpha} = C \int_0^{\infty} d\omega \frac{\eta(\omega)}{\hbar\omega} \int d^2 r_{\perp} \hat{E}''_{\alpha}{}^{\dagger}(\mathbf{r}_{\perp}; \omega) \hat{E}''_{\alpha}(\mathbf{r}_{\perp}; \omega), \quad (7)$$

where  $C = 4\pi c_0 n \epsilon_0$ , the dagger denotes Hermitian conjugation and the spatial integral covers the entire transverse profile of the probe beam. The frequency-dependent quantum efficiency of the photodetector  $\eta(\omega) \approx 1$  over the detected frequency range but vanishes quickly for  $\omega \rightarrow 0$ .

Inserting Eq. (6) into Eq. (7) and neglecting the second-order terms in  $\delta \hat{\mathbf{E}}''$  as well as the mixed terms depending linearly both on  $\delta \hat{\mathbf{E}}''$  and on  $\hat{E}_{\text{THz}}$  (contained in  $\hat{\phi}$ ) [35], we obtain for the total detected quantum signal

$$\hat{\mathcal{S}} \equiv \hat{\mathcal{N}}_s - \hat{\mathcal{N}}_z = \hat{\mathcal{S}}_{\text{eo}} + \hat{\mathcal{S}}_{\text{sn}}, \quad (8)$$

where the electro-optic signal (EOS)  $\hat{\mathcal{S}}_{\text{eo}}$  is

$$\hat{\mathcal{S}}_{\text{eo}} = C \int d^2 r_{\perp} \int_0^{\infty} d\omega \frac{\eta(\omega)}{\hbar\omega} |E_p(\mathcal{Y})|^2 \left[ \hat{\phi}(\mathcal{Y}) + \text{H.c.} \right] \quad (9)$$

and the shot noise (SN) contribution  $\hat{\mathcal{S}}_{\text{sn}}$  reads  $\hat{\mathcal{S}}_{\text{sn}} = C \int d^2 r_{\perp} \int_0^{\infty} d\omega \frac{\eta(\omega)}{\hbar\omega} \left[ E_{\text{p}}^*(\mathcal{Y}) \delta \hat{E}_+''(\mathcal{Y}) + \text{H.c.} \right]$ . Here H.c. denotes the Hermitian conjugate and  $\delta \hat{E}_+''(\mathcal{Y}) = e^{i\pi/4} [\delta \hat{E}_s''(\mathcal{Y}) + i \delta \hat{E}_z''(\mathcal{Y})] / \sqrt{2}$  is the circular component of the probe field vacuum contribution [36]. Summing up the signals from both detectors, we obtain the expectation value of the number of detected photons per probe pulse  $N = \langle \hat{\mathcal{N}}_s + \hat{\mathcal{N}}_z \rangle = \frac{4\pi c_0 n \epsilon_0}{\hbar} \int_0^{\infty} d\omega \frac{\eta(\omega)}{\omega} |\alpha_{\text{p}}(\omega)|^2$ .

Using Eqs. (3) and (5) in Eq. (9), we obtain

$$\hat{\mathcal{S}}_{\text{eo}} = \frac{dlN\omega_{\text{p}}}{c_0 n} \int d^2 r_{\perp} g_{00}^2(\mathbf{r}_{\perp}) \int_{-\infty}^{\infty} d\Omega \hat{E}_{\text{THz}}(\mathbf{r}_{\perp}; \Omega) R(\Omega). \quad (10)$$

$g_{00}(\mathbf{r}_{\perp}) \equiv \text{LG}_{00}(\mathbf{r}_{\perp}, r_{\parallel} = 0; k_{\omega}) = \sqrt{2/\pi} w_0^{-1} \exp(-r_{\perp}^2/w_0^2)$  is a normalized Gaussian independent of  $\omega$  and  $\omega_{\text{p}} = \int_0^{\infty} d\omega \eta(\omega) |\alpha_{\text{p}}(\omega)|^2 / \int_0^{\infty} d\omega \frac{\eta(\omega)}{\omega} |\alpha_{\text{p}}(\omega)|^2$  is the average detected frequency. We have introduced the response function  $R(\Omega) = \text{sinc} \left[ \frac{l\Omega}{2c_0} (n_{\Omega} - n_{\text{g}}) \right] f(\Omega)$  with the normalized Hermitian spectral autocorrelation function  $f(\Omega) = [f_+^*(\Omega) + f_-(\Omega)]/2$ , where  $f_{\pm}(\Omega) = \int_0^{\infty} d\omega \eta(\omega) \alpha_{\text{p}}^*(\omega) \alpha_{\text{p}}(\omega \pm \Omega) / \int_0^{\infty} d\omega \eta(\omega) |\alpha_{\text{p}}(\omega)|^2$ .

Within the paraxial quantization [32],  $\hat{E}_{\text{THz}}(\mathbf{r}_{\perp}; \Omega)$  in Eq. (10) is given by [25]

$$\hat{E}_{\text{THz}}(\mathbf{r}_{\perp}; \Omega) = -i \sum_{l,p} \sqrt{\frac{\hbar\Omega}{4\pi\epsilon_0 c_0 n_{\Omega}}} \hat{a}_{s,l,p}(\Omega) g'_{lp}(\mathbf{r}_{\perp}) \quad (11)$$

for  $\Omega > 0$ ,  $\hat{E}_{\text{THz}}(\mathbf{r}_{\perp}; \Omega < 0) = \hat{E}_{\text{THz}}^{\dagger}(\mathbf{r}_{\perp}; -\Omega)$ . Here,  $\hat{a}_{s,l,p}(\Omega)$  annihilates a photon with frequency  $\Omega$ , orbital quantum numbers  $l, p$  and polarization  $\mathbf{e}_s$ . We have introduced the transverse mode functions  $g'_{lp}(\mathbf{r}_{\perp}) \equiv \text{LG}_{lp}(\mathbf{r}_{\perp}, r_{\parallel} = 0; k_{\Omega})$ . In contrast to the probe beam, the waist size  $w'_0$  characterizing these mode functions is a free parameter of the expansion (11). Inserting Eq. (11) into Eq. (10) and selecting  $w'_0 = w_0/\sqrt{2}$ , we can perform the spatial integration using  $\int d^2 r_{\perp} g_{00}^2(\mathbf{r}_{\perp}) g'_{lp}(\mathbf{r}_{\perp}) = \frac{1}{\sqrt{\pi} w_0} \delta_{l,0} \delta_{p,0}$ . Then we obtain from Eq. (10)

$$\hat{\mathcal{S}}_{\text{eo}} = -i\sqrt{B} \int_0^{\infty} d\Omega \sqrt{\frac{\Omega}{n_{\Omega}}} [\hat{a}_{s,0,0}(\Omega) R(\Omega) - \text{H.c.}], \quad (12)$$

where  $B = (d^2 l^2 N^2 \omega_{\text{p}}^2 \hbar) / (4\pi^2 \epsilon_0 c_0^3 n^2 w_0^2)$ .

As an input, we now consider a THz quantum field with no coherent (classical) contribution:  $\langle \hat{E}_{\text{THz}} \rangle = 0$ , e.g., a bare multi-THz vacuum. Then  $\langle \hat{\mathcal{S}} \rangle = 0$  since  $\langle \hat{\mathcal{S}}_{\text{sn}} \rangle = 0$  and  $\hat{\phi}$  in Eq. (9) depends linearly on  $\hat{E}_{\text{THz}}$ , thus also  $\langle \hat{\mathcal{S}}_{\text{eo}} \rangle = 0$ . However, the variance of the signal does not vanish. If the range of detected THz frequencies, determined by  $R(\Omega)$ , does not overlap with the frequency content of the probe beam, the signal variance  $\langle \hat{\mathcal{S}}^2 \rangle - \langle \hat{\mathcal{S}} \rangle^2 = \langle \hat{\mathcal{S}}^2 \rangle$  can be written as  $\langle \hat{\mathcal{S}}^2 \rangle = \langle \hat{\mathcal{S}}_{\text{eo}}^2 \rangle + \langle \hat{\mathcal{S}}_{\text{sn}}^2 \rangle$ . Calculating the SN contribution using the paraxial quantization [32], we obtain the expected result  $\langle \hat{\mathcal{S}}_{\text{sn}}^2 \rangle = N$ .

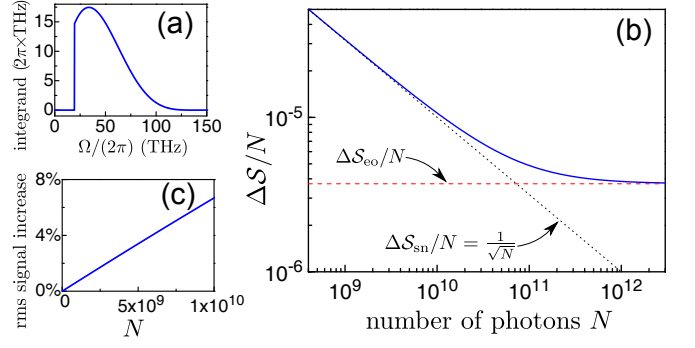


FIG. 2. (color online) (a) Calculated integrand function  $\Omega(n/n_{\Omega})|R(\Omega)|^2$  entering Eq. (13). (b) Double-logarithmic plot of the ratio  $\Delta S/N$  in dependence on  $N$ . Black dotted (red dashed) line shows the bare SN (multi-THz vacuum) contribution. (c) Increase of  $(\Delta S - \Delta S_{\text{sn}})/\Delta S_{\text{sn}}$  with  $N$ . Parameters are defined in the main text.

Evaluating  $\langle \hat{\mathcal{S}}_{\text{eo}}^2 \rangle$  for the multi-THz vacuum yields

$$\langle \hat{\mathcal{S}}_{\text{eo}}^2 \rangle = N^2 \left( n^3 \frac{l\omega_{\text{p}}}{c_0} r_{41} \right)^2 \frac{\hbar \int_0^{\infty} d\Omega \Omega (n/n_{\Omega}) |R(\Omega)|^2}{4\pi^2 \epsilon_0 c_0 n w_0^2} \quad (13)$$

where we have used  $\langle \hat{a}_{s,0,0}(\Omega) \hat{a}_{s,0,0}^{\dagger}(\Omega') \rangle = \delta(\Omega - \Omega')$ , whereas the expectation values of other possible quadratic combinations of  $\hat{a}_{s,l,p}^{\dagger}$  and  $\hat{a}_{s,l,p}$  vanish. Note that the second and third factors on the right-hand side of Eq. (13) have the dimensions  $(\text{m/V})^2$  and  $(\text{V/m})^2$ , respectively. The latter can be interpreted as the square of the effective multi-THz rms (root mean square) vacuum electric field filtered by the response function. The former,  $\propto r_{41}^2$ , determines how effectively this field is sampled for a fixed  $N$ .

To illustrate the results, we assume the following realistic specifications of the sampling few-femtosecond NIR laser pulse: center frequency 255 THz, spectral bandwidth 150 THz with rectangular spectral shape and flat phase, leading to  $\omega_{\text{p}} = 247$  THz, and waist size  $w_0 = 3 \mu\text{m}$  [37]. We consider a  $l = 7 \mu\text{m}$  thick ZnTe EOX with  $r_{41} = 4 \text{ pm/V}$  [38, 39],  $n = 2.76$ ,  $n_{\text{g}} = 2.9$ , and  $n_{\Omega}$  varying only slightly (from 2.55 to 2.59) for relevant THz frequencies [25]. The resulting integrand function entering Eq. (13) is shown in Fig. 2(a) (for details, see Ref. [25]). Diffraction effects are taken into account by excluding wavelengths  $\lambda$  with  $\lambda/(2n_{\Omega}) > w_0$ .

Based on this input, we calculate the dependence of the rms value of the signal  $\Delta S = \langle \hat{\mathcal{S}}^2 \rangle^{1/2}$  on the average number  $N$  of photons in the sampling NIR pulse, as shown in Fig. 2(b) on a double-logarithmic scale. Above a certain  $N$ , the EOS contribution of the multi-THz vacuum changes the typical SN scaling. The relative increase of the rms value of the signal with respect to the SN level,  $(\Delta S - \Delta S_{\text{sn}})/\Delta S_{\text{sn}}$ , is depicted in Fig. 2(c) for moderate  $N$  and with linear scaling. For even higher  $N$ , the vacuum contribution starts to dominate so that the dependence saturates to the constant EOS level [Fig. 2(b)].

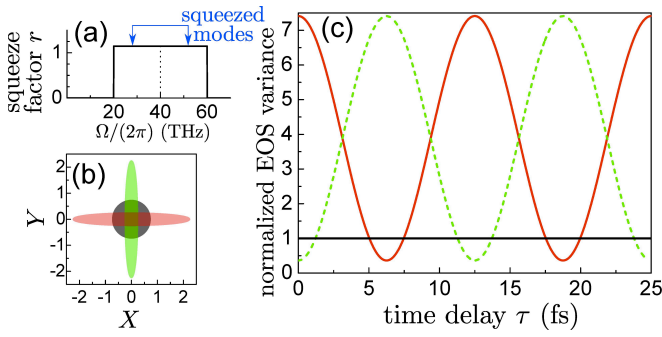


FIG. 3. (color online) (a) Frequency dependence of the squeeze factor  $r$ . Squeezing correlates  $\Omega$  and  $2\Omega_c - \Omega$  modes (as indicated by arrows). (b) Error contour in the complex-amplitude plane for PV (gray circle) and SV with  $\theta=0/\theta=\pi$  (red/green ellipse with reduced uncertainty in the phase/amplitude quadrature  $Y/X$ ). (c) Normalized (with respect to the constant PV level, solid black line) EOS variance in dependence on the time delay  $\tau$  of the probe NIR pulse for SV with  $\theta=0/\theta=\pi$  (solid red line / dashed green line).

Subtracting the SN contribution from the total signal variance, the bare EOS variance induced by the sampled quantum field can be obtained and analyzed.

To elaborate on this point, we apply our theory to a multi-THz vacuum which is squeezed in an interval around a central frequency  $\Omega_c$ . The corresponding state of light is obtained by applying the continuum squeezing operator [40–42]  $\exp\left[\frac{1}{2}\int_0^{2\Omega_c} d\Omega \sum_{\alpha l p} (\xi_{\Omega}^* \hat{a}_{\alpha, l, p}(2\Omega_c - \Omega) \hat{a}_{\alpha, l, p}(\Omega) - \text{H.c.})\right]$  to the multi-THz pure vacuum (PV) state considered above. Here the frequency-dependent squeezing parameter  $\xi(\Omega)$  satisfies the condition  $\xi(\Omega) = \xi(2\Omega_c - \Omega)$ . We assume that all spatial and polarization modes are squeezed equally. In this case, the EOS can be obtained from Eq. (12) applying the transformation  $\hat{a}_{s,0,0}(\Omega) \rightarrow \hat{a}_{s,0,0}(\Omega) \cosh r_{\Omega} - \hat{a}_{s,0,0}^{\dagger}(2\Omega_c - \Omega) e^{i\theta} \sinh r_{\Omega}$  [40–42] and working in the vacuum picture. The expectation value of the signal remains zero. Evaluation of the EOS variance for the squeezed vacuum (SV),  $\langle \hat{\mathcal{S}}_{\text{eo}}^2 \rangle_{\text{sv}}(\tau)$ , is analogous to the PV case. However, the SV EOS variance depends on the time delay  $\tau$  of the NIR probe pulse leading to the transformation  $R(\Omega) \rightarrow R(\Omega) e^{-i\Omega\tau}$  of the response function, a fact that was unimportant for handling the PV [cf. Eq. (13)]. For a probe pulse symmetric with respect to  $t = \tau$ , i.e.  $E_p(t - \tau) = E_p(\tau - t)$ , we find  $R(\Omega) = R_0(\Omega) e^{-i\Omega\tau}$ , where  $R_0(\Omega)$  is real-valued.

For our illustration we assume constant squeezing with  $\xi(\Omega) \equiv \xi = r e^{i\theta}$  in the frequency range  $[\Omega_1, \Omega_2]$  with  $\Omega_c = (\Omega_1 + \Omega_2)/2$ , where  $r = |\xi|$  is the squeeze factor [43, 44] and  $\theta = \text{Arg}(\xi)$  is the squeezing phase [41]. No squeezing occurs outside this range. In particular, we use  $\Omega_c/(2\pi) = 40$  THz,  $\Omega_2 - \Omega_1 = \Omega_c$  and  $\sinh r = 2$  [see Fig. 3(a)]. Generalized quadrature operators [40]  $\hat{X}_{\lambda} =$

$\frac{1}{\sqrt{2(\Omega_2 - \Omega_1)}} \int_{\Omega_1}^{\Omega_2} d\Omega [\hat{a}_{s,0,0}(\Omega) e^{-i\lambda} + \text{H.c.}]$ , with  $\hat{X} = \hat{X}_0$  and  $\hat{Y} = \hat{X}_{\pi/2}$ , normalized so that  $[\hat{X}, \hat{Y}] = i$  are introduced. The error contours for PV as well as for SV as described above and two different squeezing phases,  $\theta = 0$  and  $\theta = \pi$ , are featured in Fig. 3(b). The dependence of the normalized EOS variance  $\langle \hat{\mathcal{S}}_{\text{eo}}^2 \rangle_{\text{sv}}(\tau) / \langle \hat{\mathcal{S}}_{\text{eo}}^2 \rangle$ , where  $\langle \hat{\mathcal{S}}_{\text{eo}}^2 \rangle$  is given by Eq. (13), on the time delay  $\tau$  is shown in Fig. 3(c) for the same states as in Fig. 3(b) and sampling parameters used for the PV case. For specific delay times, the EOS variance of the multi-THz SV is by 64% lower than the unsqueezed value of the PV state (for details, see Ref. [25]).

We emphasize the cardinal difference between our findings and similar-looking results obtained in the context of homodyning [45, 46]. In homodyning experiments, the signal is determined by the temporal overlap integral of the *complex amplitudes* of the electric fields of an input state and a local oscillator, i.e. the information is essentially averaged over multiple oscillation cycles of light. A restricted frequency bandwidth has to be assumed to justify the slowly varying amplitude approximation underlying this approach. In contrast, electro-optic sampling provides a true sub-cycle resolution of the probed multi-THz *electric field*. Moreover, registration of photons is transferred into the NIR, circumventing the lack of efficient single-photon detectors in the multi-THz frequency range. Most importantly, the multi-THz quantum field may be studied without the necessity to reduce or amplify its photon content - even if it remains in its ground state.

In conclusion, we theoretically clarify the contribution of the quantum fluctuations of the multi-THz vacuum electric field to the signal in ultrabroadband electro-optic sampling by differentiating it from the trivial shot noise of the high-frequency gating pulse. The crucial aspects are a strong localization of the sampling beam in space and time as it passes the nonlinear crystal, a large second-order nonlinear coefficient and proper phase matching that might be further optimized selecting an even more appropriate material than the thin piece of ZnTe we have considered as an example. For a multi-THz squeezed vacuum, the possibility to trace the oscillations of the EOS variance with the time delay of the probe pulse is predicted. Positions occur where the noise remains significantly below the level of unsqueezed vacuum. The same formalism can be applied for the analysis of more complex quantum fields in a time-resolved and non-destructive manner. Experimental implementation of these ideas might open up a new chapter of quantum optics operating predominantly in the time domain and with access to sub-cycle information on the quantum state of electromagnetic radiation.

We acknowledge funding from the ERC via the Advanced Grant 290876 “UltraPhase” and by DFG within SFB 767. We thank M. Kira for useful discussions.

- 
- \* andrey.moskalenko@physik.uni-konstanz.de
- [1] J. J. Sakurai, *Advanced Quantum Mechanics* (Addison-Wesley, 1967).
  - [2] W. E. Lamb and R. C. Retherford, *Phys. Rev.* **72**, 241 (1947).
  - [3] A. Fragner, M. Goppl, J. M. Fink, M. Baur, R. Bianchetti, P. J. Leek, A. Blais, and A. Wallraff, *Science* **322**, 1357 (2008).
  - [4] R. Hanbury Brown and R. Q. Twiss, *Nature (London)* **177**, 27 (1956).
  - [5] H. J. Kimble, M. Dagenais, and L. Mandel, *Phys. Rev. Lett.* **39**, 691 (1977).
  - [6] J. Shapiro, H. P. Yuen, and A. Mata, *IEEE Trans. Inf. Theory* **25**, 179 (1979).
  - [7] L. Mandel, *Phys. Rev. Lett.* **49**, 136 (1982).
  - [8] R. E. Slusher, L. W. Hollberg, B. Yurke, J. C. Mertz, and J. F. Valley, *Phys. Rev. Lett.* **55**, 2409 (1985).
  - [9] D. T. Smithey, M. Beck, M. G. Raymer, and A. Faridani, *Phys. Rev. Lett.* **70**, 1244 (1993).
  - [10] G. Breitenbach, S. Schiller, and J. Mlynek, *Nature (London)* **387**, 471 (1997).
  - [11] C. Silberhorn, *Contemp. Phys.* **48**, 143 (2007).
  - [12] D. H. Auston, K. P. Cheung, and P. R. Smith, *Appl. Phys. Lett.* **45**, 284 (1984).
  - [13] Ch. Fattinger and D. Grischkowsky, *Appl. Phys. Lett.* **54**, 490 (1989).
  - [14] D. H. Auston, *Appl. Phys. Lett.* **26**, 101 (1975).
  - [15] Q. Wu and X. Zhang, *Appl. Phys. Lett.* **67**, 3523 (1995).
  - [16] A. Nahata, A. S. Weling, and T. F. Heinz, *Appl. Phys. Lett.* **69**, 2321 (1996).
  - [17] G. Gallot and D. Grischkowsky, *J. Opt. Soc. Am. B* **16**, 1204 (1999).
  - [18] K. Liu, J. Xu, and X.-C. Zhang, *Appl. Phys. Lett.* **85**, 863 (2004).
  - [19] C. Kübler, R. Huber, S. Tübel, and A. Leitenstorfer, *Appl. Phys. Lett.* **85**, 3360 (2004).
  - [20] D. N. Basov, R. D. Averitt, D. van der Marel, M. Dressel, and K. Haule, *Rev. Mod. Phys.* **83**, 471 (2011).
  - [21] R. Ulbricht, E. Hendry, J. Shan, T. F. Heinz, and M. Bonn, *Rev. Mod. Phys.* **83**, 543 (2011).
  - [22] R. Kienberger, E. Goulielmakis, M. Uiberacker, A. Baltuska, V. Yakovlev, F. Bammer, A. Scrinzi, T. Westerwalbesloh, U. Kleineberg, U. Heinzmann, M. Drescher, and F. Krausz, *Nature (London)* **427**, 817 (2004).
  - [23] P. C. M. Planken, H.-K. Nienhuys, H. J. Bakker, and T. Wenckebach, *J. Opt. Soc. Am. B* **18**, 313 (2001).
  - [24] S. Namba, *J. Opt. Soc. Am.* **51**, 76 (1961).
  - [25] See Supplemental Material at [URL will be inserted by publisher] for details.
  - [26] G. New, *Introduction to Nonlinear Optics* (Cambridge University Press, New York, 2011).
  - [27] P. E. Powers, *Fundamentals of Nonlinear Optics* (Taylor & Francis, Boca Raton, 2011).
  - [28] A. Yariv, *Quantum Electronics* (John Wiley & Sons, New York, 1989).
  - [29] R. W. Boyd, *Nonlinear Optics (Third Edition)* (Academic Press, Burlington, 2008).
  - [30] Y. R. Shen, *Principles of nonlinear optics* (Wiley-Interscience, New York, 1984).
  - [31] L. Allen, M. W. Beijersbergen, R. J. C. Spreeuw, and J. P. Woerdman, *Phys. Rev. A* **45**, 8185 (1992).
  - [32] G. F. Calvo, A. Picón, and E. Bagan, *Phys. Rev. A* **73**, 013805 (2006).
  - [33] P. Knight and L. Allen, *Concepts of Quantum Optics* (Pergamon Press, Oxford, 1983).
  - [34] Confer Ref. [47] for a case with a simpler transverse mode structure.
  - [35] The mixed terms were also neglected already in Eq. (1). The second order terms in  $\delta\hat{\mathbf{E}}''$  ( $\delta\hat{E}_z''\delta\hat{E}_z''$  and  $\delta\hat{E}_s''\delta\hat{E}_s''$ ) do not contribute to the expectation value of the signal, neither to its variance or any higher moments.
  - [36] The phase shift is of no physical importance for the vacuum field contribution.
  - [37] D. Brida, G. Krauss, A. Sell, and A. Leitenstorfer, *Laser Photon. Rev.* **8**, 409 (2014).
  - [38] A. Cingolani, M. Ferrara, and M. Lugarà, *Solid State Commun.* **38**, 819 (1981).
  - [39] A. Leitenstorfer, S. Hunsche, J. Shah, M. C. Nuss, and W. H. Knox, *Appl. Phys. Lett.* **74**, 1516 (1999).
  - [40] S. Barnett and P. Radmore, *Methods in Theoretical Quantum Optics*, Oxford Series in Optical and Imaging Sciences (Oxford University Press, New York, 2002).
  - [41] W. Vogel and D. Welsch, *Quantum Optics* (Wiley, Weinheim, 2006).
  - [42] K. J. Blow, R. Loudon, S. J. D. Phoenix, and T. J. Shepherd, *Phys. Rev. A* **42**, 4102 (1990).
  - [43] C. M. Caves, *Phys. Rev. D* **23**, 1693 (1981).
  - [44] D. Walls and G. Milburn, *Quantum Optics* (Springer, Berlin, 2008).
  - [45] M. E. Anderson, D. F. McAlister, M. G. Raymer, and M. C. Gupta, *J. Opt. Soc. Am. B* **14**, 3180 (1997).
  - [46] R. E. Slusher, P. Grangier, A. LaPorta, B. Yurke, and M. J. Potasek, *Phys. Rev. Lett.* **59**, 2566 (1987).
  - [47] M. G. Raymer, J. Cooper, H. J. Carmichael, M. Beck, and D. T. Smithey, *J. Opt. Soc. Am. B* **12**, 1801 (1995).

## Supplemental Material

### Paraxial Theory of Direct Electro-Optic Sampling of the Quantum Vacuum

A.S. Moskalenko, C. Riek, D.V. Seletskiy, G. Burkard, and A. Leitenstorfer

#### 1. GEOMETRY OF NONLINEAR MIXING

For the nonlinear mixing in the EOX, we select the orientation of  $\mathbf{E}_p$  parallel to the  $z$ -axis. This choice of the polarization direction of the probe field ensures that the maximum signal is detected in the electro-optic detection scheme for a copropagating classical THz electric field polarized perpendicular to the probe electric field [S1]. In the experiment, adjustment is achieved by rotation of the EOX around the [110] axis for fixed, mutually perpendicular polarization directions of the probe and detected electric fields. Also, only one of two possible polarization modes of the detected field [the one perpendicular to the probe field, i.e. oriented parallel to the unit vector  $\mathbf{e}_s$  in Fig. 1(b)] contributes to the signal in this geometry. There is no THz field generated by optical rectification of the probe for this orientation of the EOX.

The second-order nonlinear mixing of the probe field  $\mathbf{E}_p(t)$  with the detected THz field  $\mathbf{E}_{\text{THz}}(t)$  then induces nonlinear polarization in the EOX with the following components [S2–S4]:

$$P_x^{(2)}(t) = 4\epsilon_0 d_{xyz} E_{\text{THz},y}(t) E_{p,z}(t) \quad (\text{S1})$$

and similarly for the  $y$ -component with the interchange of indices  $x \leftrightarrow y$  in Eq. (S1). Here  $\epsilon_0$  is the vacuum permittivity. For the zincblende-type EOX we adopt as an example, the tensor components  $d_{xyz} \equiv \chi_{xyz}^{(2)}/2$  and  $d_{yxz} \equiv \chi_{yxz}^{(2)}/2$  are both equal to the same constant denoted by  $d_{36}$  [S2–S4]. This coefficient is related to the constant  $r_{41}$  used for the description of the Pockels effect as  $d_{36} = -n^4 r_{41}/4$ .  $n$  is the refractive index at the central frequency of the probe electric field. For the following discussion, it is convenient to introduce  $d = 4d_{36} = -n^4 r_{41}$ . Writing Eq. (S1) as an instantaneous relation in the time domain we assume that the frequencies  $\Omega$  of the THz field are lower than the frequencies  $\omega$  of the probe field and that the second-order nonlinear coefficient can be considered constant in the frequency range determined by the spectral width of the probe field. The frequency dependence of the nonlinear coefficient can be easily included writing the corresponding equations in the frequency domain, similar to Ref. [S5] but taking care of the particular geometry. However, the discussion of the geometrical issues is more concise in the time domain whereas the effect of the frequency dependence of the nonlinear coefficient is finally not significant in our case.

The nonlinear polarization induced in the (110) plane is given by  $\mathbf{P}^{(2)} = \frac{1}{\sqrt{2}}(P_y^{(2)} - P_x^{(2)})\mathbf{e}_s$ , i.e.  $P_z^{(2)} = 0$  and  $P_s^{(2)} = \frac{1}{\sqrt{2}}(P_y^{(2)} - P_x^{(2)})$ , using the unit vectors  $\mathbf{e}_s$  and  $\mathbf{e}_z$  as a basis in this plane. Taking Eq. (S1), expressing also the components of the quantized THz field in this basis and neglecting the effect of quantum mechanical fluctuations of the probe beam on the induced nonlinear polarization, i.e. assuming a sufficiently strong probe field, we arrive at Eq. (1). Inclusion of the vacuum contribution for the probe beam at this place would mean taking into account mixed second-order corrections linearly dependent on both the vacuum fluctuations of the probe field and on the probed THz field. In our present consideration, we neglect such terms since they do not lead to significant effects.

#### 2. LAGUERRE-GAUSSIAN MODES AND PARAXIAL ELECTROMAGNETIC FIELD QUANTIZATION

In electro-optic sampling, propagation of the NIR probe beam through the EOX can be well described within the paraxial approximation. The same approximation can be naturally used to describe the sampled multi-THz quantum fields. The corresponding expression for a quantized electric field within the paraxial approximation was derived in Ref. [S6]. In free space, with the propagation axis selected as shown in Fig. 1, it reads

$$\hat{\mathbf{E}}(\mathbf{r}, t) = -i \sum_{\alpha, l, p} \int_0^\infty dk \sqrt{\frac{\hbar \Omega}{4\pi \epsilon_0}} \left[ \mathbf{e}_\alpha \hat{a}_{\alpha, l, p}(k) e^{i(kr_\parallel - \Omega t)} \text{LG}_{lp}(\mathbf{r}_\perp, r_\parallel; k) - \text{H.c.} \right], \quad (\text{S2})$$

where  $\hat{a}_{\alpha, l, p}(k)$  denotes the annihilation operator for a photon with absolute value of the wave vector  $k$ , frequency  $\Omega = c_0 k$ , orbital quantum numbers  $l, p$ , and polarization direction  $\mathbf{e}_\alpha$ . The spatial mode functions are given by the

Laguerre-Gaussian (LG) modes  $\text{LG}_{lp}(\mathbf{r}_\perp, r_\parallel; k) \equiv \text{LG}_{lp}(r_\perp, \varphi, r_\parallel; k)$  which can be written as [S6, S7]

$$\text{LG}_{lp}(r_\perp, \varphi, r_\parallel; k) = \sqrt{\frac{2p!}{\pi(|l|+p)!}} \frac{1}{w(r_\parallel)} \left( \frac{\sqrt{2}r_\perp}{w(r_\parallel)} \right)^{|l|} L_p^{|l|} \left( \frac{2r_\perp^2}{w^2(r_\parallel)} \right) \exp \left[ -\frac{2r_\perp^2}{w^2(r_\parallel)} + il\varphi + i\frac{kr_\perp^2}{2\mathcal{R}(r_\parallel)} + i\Phi_G(r_\parallel) \right]. \quad (\text{S3})$$

Here  $w(r_\parallel) = w_0 \sqrt{1 + r_\parallel^2/l_R^2(\Omega)}$  is the transverse mode radius at the longitudinal position  $r_\parallel$  with  $w_0$  being the waist size of the probe beam (mode radius at  $r_\parallel = 0$ ) and  $l_R(\Omega) = kw_0^2/2$  denoting the Rayleigh range of the beam at given  $k$ .  $\mathcal{R}(r_\parallel) = r_\parallel \left[ 1 + l_R^2(\Omega)/r_\parallel^2 \right]$  is the phase-front radius,  $\Phi_G(r_\parallel) = -(2p + |l| + 1) \arctan(r_\parallel/w_0)$  is the Gouy phase and  $L_p^{|l|}(x)$  are the associated Laguerre polynomials [S8]. The LG modes are normalized such that  $\int_0^{2\pi} d\phi \int_0^\infty dr_\perp r_\perp \text{LG}_{lp}^*(r_\perp, \phi, r_\parallel; k) \text{LG}_{l'p'}(r_\perp, \phi, r_\parallel; k) = \delta_{ll'} \delta_{pp'}$  (for any  $k$  and  $r_\parallel$ ), where  $\delta_{ij}$  denotes the Kronecker delta. The annihilation and creation operators satisfy the continuum commutation relations  $[\hat{a}_{\alpha,l,p}(k), \hat{a}_{\alpha',l',p'}(k')] = [\hat{a}_{\alpha,l,p}^\dagger(k), \hat{a}_{\alpha',l',p'}^\dagger(k')] = 0$  and  $[\hat{a}_{\alpha,l,p}(k), \hat{a}_{\alpha',l',p'}^\dagger(k')] = \delta_{\alpha\alpha'} \delta_{ll'} \delta_{pp'} \delta(k - k')$ . Expressing the creation and annihilation operators as functions of frequency, whereby they satisfy  $[\hat{a}_{\alpha,l,p}(\Omega), \hat{a}_{\alpha',l',p'}(\Omega')] = [\hat{a}_{\alpha,l,p}^\dagger(\Omega), \hat{a}_{\alpha',l',p'}^\dagger(\Omega')] = 0$  and  $[\hat{a}_{\alpha,l,p}(\Omega), \hat{a}_{\alpha',l',p'}^\dagger(\Omega')] = \delta_{\alpha\alpha'} \delta_{ll'} \delta_{pp'} \delta(\Omega - \Omega')$ , Eq. (S2) transforms into

$$\hat{\mathbf{E}}(\mathbf{r}, t) = -i \sum_{\alpha,l,p} \int_0^\infty d\Omega \sqrt{\frac{\hbar\Omega}{4\pi\epsilon_0 c_0}} \left[ \mathbf{e}_\alpha \hat{a}_{\alpha,l,p}(\Omega) e^{i(k_\Omega r_\parallel - \Omega t)} \text{LG}_{lp}(\mathbf{r}_\perp, r_\parallel; k_\Omega) - \text{H.c.} \right]. \quad (\text{S4})$$

By writing  $k_\Omega$  we have stressed that we consider  $k \equiv k_\Omega = \Omega/c_0$  as a function of  $\Omega$  in this expression. Note that the factor of  $16\pi^3$  in the denominator under the square root in Eq. (20) of Ref. [S6] needs to be replaced by  $4\pi$ . This fact is confirmed by deriving the expression for the total energy operator of the electro-magnetic field and has been considered in Eq. (S2). From Eq. (S4), the total energy operator  $\hat{\mathcal{E}}$  is obtained in its correct form as  $\hat{\mathcal{E}} = \int_0^\infty d\Omega \hbar\Omega \sum_{\alpha,l,p} \hat{a}_{\alpha,l,p}^\dagger(\Omega) \hat{a}_{\alpha,l,p}(\Omega)$ .

In media with refractive index  $n_\Omega$ , the factor under the square root in Eq. (S4) should be additionally divided by  $n_\Omega$  [S9, pp. 391-392]. This measure again ensures a correct expression for the total energy operator of the field so that Eq. (S4) takes the form

$$\hat{\mathbf{E}}(\mathbf{r}, t) = -i \sum_{\alpha,l,p} \int_0^\infty d\Omega \sqrt{\frac{\hbar\Omega}{4\pi\epsilon_0 c_0 n_\Omega}} \left[ \mathbf{e}_\alpha \hat{a}_{\alpha,l,p}(\Omega) e^{i(k_\Omega r_\parallel - \Omega t)} \text{LG}_{lp}(\mathbf{r}_\perp, r_\parallel; k_\Omega) - \text{H.c.} \right]. \quad (\text{S5})$$

When we consider a thin EOX located at the beam waist ( $r_\parallel = 0$ ), we use  $\text{LG}_{lp}(\mathbf{r}_\perp, r_\parallel; k) \approx \text{LG}_{lp}(\mathbf{r}_\perp, r_\parallel = 0; k) \equiv g_{lp}(\mathbf{r}_\perp)$ , which are given by

$$g_{lp}(\mathbf{r}_\perp) = \sqrt{\frac{2p!}{\pi(|l|+p)!}} \frac{1}{w_0} \left( \frac{\sqrt{2}r_\perp}{w_0} \right)^{|l|} L_p^{|l|} \left( \frac{2r_\perp^2}{w_0^2} \right) \exp \left( -\frac{r_\perp^2}{w_0^2} + il\varphi \right). \quad (\text{S6})$$

The transverse modes  $g_{lp}(\mathbf{r}_\perp) \equiv g_{lp}(r_\perp, \phi)$  are independent of  $k$ . They are normalized such that

$$\int_0^{2\pi} d\phi \int_0^\infty dr_\perp r_\perp g_{lp}^*(r_\perp, \phi) g_{l'p'}(r_\perp, \phi) = \delta_{l,l'} \delta_{p,p'}.$$

The fundamental (lowest-order) mode is Gaussian-shaped and given by

$$g_{00}(\mathbf{r}_\perp) = \sqrt{\frac{2}{\pi}} \frac{1}{w_0} \exp \left( -\frac{r_\perp^2}{w_0^2} \right). \quad (\text{S7})$$

When the EOX is located at  $r_\parallel \neq 0$ , the same approximation applies and one can proceed similarly, just changing  $w_0 \rightarrow w(r_\parallel)$  in the expressions for  $g_{lp}(\mathbf{r}_\perp)$ .

### 3. REFRACTIVE INDICES AND RESPONSE FUNCTION

In the paper we used a sampling few-femtosecond NIR laser pulse of the following specifications [S10]: center frequency  $\omega_c/(2\pi) = 255$  THz, spectral bandwidth  $\Delta\omega/(2\pi) = 150$  THz with rectangular spectral shape and flat

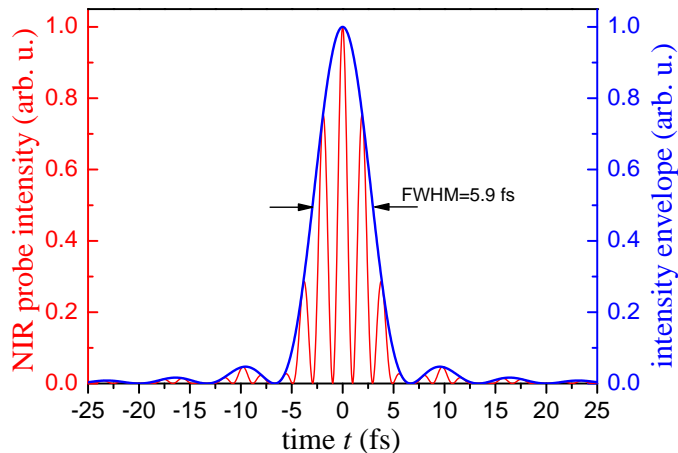


FIG. S1. Temporal profile of the intensity (red line) and its envelope (blue line) of the NIR probe pulse used in our calculations.

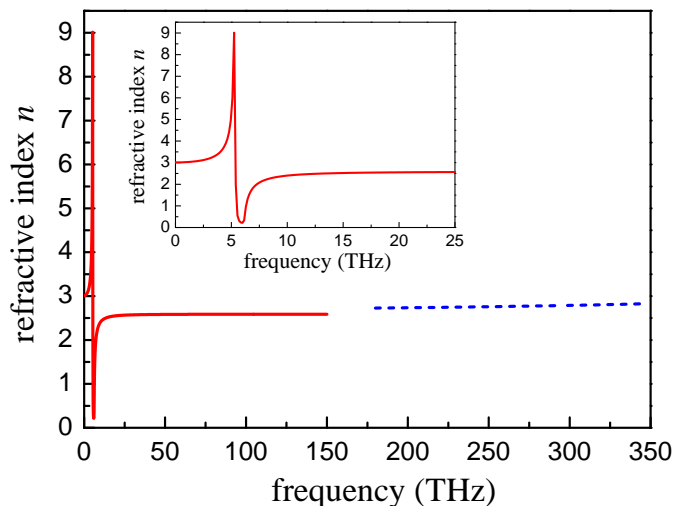


FIG. S2. Dispersion of the refractive index in the THz (solid red line) and NIR (dashed blue line) range. Inset shows the dispersion with a higher frequency resolution in the range of small THz frequencies.

phase. The corresponding temporal profile of the NIR probe intensity is shown in Fig. S1. For such a pulse we get  $\omega_p = 247$  THz, where  $\omega_p$  is defined in the text after Eq. (10). Notice that  $\omega_p \approx \omega_c$ . However, there is a small difference in these quantities due to different averaging used in their definitions. This difference is of minor importance for our consideration. The normalized Hermitian spectral autocorrelation function  $f(\Omega)$ , as defined in the text after Eq. (10), can be found as

$$f(\Omega) = \left(1 - \frac{|\Omega|}{\Delta\omega}\right) H(\Delta\omega - |\Omega|), \quad (\text{S8})$$

where  $H(x)$  denotes the Heaviside step function. For our example with a rectangular probe spectrum,  $f(\Omega)$  takes the shape of an isosceles triangle with the vertex at  $\Omega = 0$ . In order to determine the response function  $R(\Omega)$ , we have to multiply  $f(\Omega)$  by the phase-matching function  $\text{sinc}\left[\frac{i\Omega}{2c_0}(n_\Omega - n_g)\right]$ . The latter requires knowledge about the refractive index  $n_\Omega$  in the THz range and group refractive index  $n_g$  at the (NIR) central frequency  $\omega_c$  of the probe pulse.

Refractive index properties of a ZnTe crystal in the NIR frequency range are modelled by a Sellmeier formula [S11]

$$n_\omega^2 = A + [B\lambda^2/(\lambda^2 - c^2)], \quad (\text{S9})$$

with  $\lambda = 2\pi c_0/\Omega$ ,  $A = 4.27$ ,  $B = 3.01$ , and  $c^2 = 0.142$  [S12]. The corresponding frequency dependence is shown on the right side of Fig. S2. For the refractive index  $n_\Omega$  in the THz frequency range, we use the parametrization from

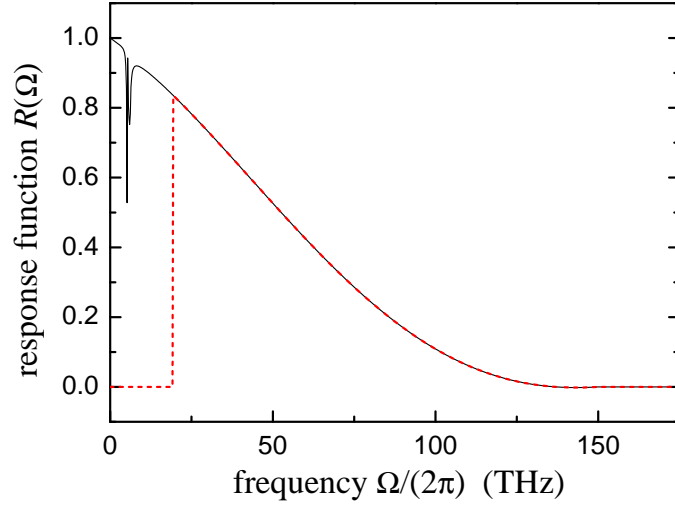


FIG. S3. Calculated response function  $R(\Omega)$  without the low-frequency cutoff (solid black line) and with the low-frequency cutoff (dashed red line).

Ref. [S13]:

$$n_{\Omega} = \text{Re} \left( \sqrt{1 + \frac{(\hbar\omega_{\text{LO}})^2 - (\hbar\omega_{\text{TO}})^2}{(\hbar\omega_{\text{TO}})^2 - (\hbar\Omega)^2 - i\hbar\gamma\Omega}} \epsilon_{\infty} \right), \quad (\text{S10})$$

with  $\hbar\omega_{\text{TO}} = 177 \text{ cm}^{-1}$ ,  $\hbar\omega_{\text{LO}} = 206 \text{ cm}^{-1}$ ,  $\gamma = 3.01 \text{ cm}^{-1}$ , and  $\epsilon_{\infty} = 6.7$ . The corresponding frequency dependence is shown on the left side of Fig. S2. From these models we obtain the following values of the refractive index and the group refractive index at  $\omega_c = 255 \text{ THz}$ :  $n = 2.76$  and  $n_g = 2.9$ . It is important that these indices are almost constant in the neighborhood of  $\omega_c$ . Using the calculated  $n_{\Omega}$  and  $n_g$  in the phase-matching function with  $l = 7 \mu\text{m}$ , the response function  $R(\Omega)$  depicted in Fig. S3 results. As discussed in the text of the paper, we introduce a low-frequency cutoff excluding wavelengths  $\lambda$  with  $\lambda/(2n_{\Omega}) > w_0$ , in order to take into account diffraction losses. The modified response function is also shown in Fig. S3. The resulting integrand function entering the integral in Eq. (13) is found in Fig. 2(a) of the paper. Note that without introducing the low-frequency cutoff we would get just a small increase of approximately 21% for the EOS variance calculated from Eq. (13).

#### 4. EOS VARIANCE FOR THE SQUEEZED MULTI-THZ VACUUM

For the EOS variance  $\langle \hat{\mathcal{S}}_{\text{eo}}^2 \rangle_{\text{sv}}(\tau)$  normalized with respect to the EOS variance of the pure vacuum  $\langle \hat{\mathcal{S}}_{\text{eo}}^2 \rangle$ , given by Eq. (13), we obtain

$$\langle \hat{\mathcal{S}}_{\text{eo}}^2 \rangle_{\text{sv}}(\tau) / \langle \hat{\mathcal{S}}_{\text{eo}}^2 \rangle = 1 + 2aM + 2b\sqrt{M(M+1)} \cos(\theta - 2\Omega_c\tau). \quad (\text{S11})$$

Here  $M = \sinh r$ ,  $a = I_a/I$ , and  $b = I_b/I$ , where

$$I = \int_0^{\infty} d\Omega \varrho^2(\Omega), \quad (\text{S12})$$

$$I_a = \int_{\Omega_1}^{\Omega_2} d\Omega \varrho^2(\Omega), \quad (\text{S13})$$

$$I_b = \int_{\Omega_1}^{\Omega_2} d\Omega \varrho(\Omega)\varrho(2\Omega_c - \Omega), \quad (\text{S14})$$

with  $\varrho(\Omega) = \sqrt{\Omega/n_{\Omega}} R_0(\Omega)$ . The real coefficients  $a$  and  $b$  generally satisfy the Cauchy-Bunyakovsky-Schwarz inequality  $b \leq a$ . Obviously, also  $a \leq 1$  is valid. The dependence of  $\langle \hat{\mathcal{S}}_{\text{eo}}^2 \rangle_{\text{sv}}(\tau) / \langle \hat{\mathcal{S}}_{\text{eo}}^2 \rangle$  on the time delay  $\tau$  is shown in Fig. 3(c) for the same states as in Fig. 3(b) and sampling parameters used for the pure vacuum case. We clearly see that

for certain delay times the EOS variance of the squeezed multi-THz vacuum can beat the uncertainty limit set by the pure vacuum state. Here, for  $M \equiv \sinh r = 2$ , its minimum value constitutes  $\approx 36\%$  of the pure vacuum level. For the selected parameters, a slightly stronger suppression of the quantum noise down to 34% can be achieved by increasing  $M$  to  $\approx 5.8$ , whereas the maximal noise is more than doubled. These values are generally determined by the coefficients  $a$  and  $b$ , introduced above, for which we have  $b < a < 1$  in the considered case. Here, due to the limitation set by this inequality, a complete noise suppression in the EOS variance is impossible for any time delay.

---

\* andrey.moskalenko@physik.uni-konstanz.de

- [S1] P. C. M. Planken, H.-K. Nienhuys, H. J. Bakker, and T. Wenckebach, *J. Opt. Soc. Am. B* **18**, 313 (2001).
- [S2] G. New, *Introduction to Nonlinear Optics* (Cambridge University Press, New York, 2011).
- [S3] P. E. Powers, *Fundamentals of Nonlinear Optics* (Taylor & Francis, Boca Raton, 2011).
- [S4] A. Yariv, *Quantum Electronics* (John Wiley & Sons, New York, 1989).
- [S5] G. Gallot and D. Grischkowsky, *J. Opt. Soc. Am. B* **16**, 1204 (1999).
- [S6] G. F. Calvo, A. Picón, and E. Bagan, *Phys. Rev. A* **73**, 013805 (2006).
- [S7] L. Allen, M. W. Beijersbergen, R. J. C. Spreeuw, and J. P. Woerdman, *Phys. Rev. A* **45**, 8185 (1992).
- [S8] M. Abramowitz and I. Stegun, *Handbook of Mathematical Functions: with Formulas, Graphs, and Mathematical Tables* (Dover, New York, 2012).
- [S9] R. Loudon, *The Quantum Theory of Light* (Oxford University Press, New York, 2000).
- [S10] D. Brida, G. Krauss, A. Sell, and A. Leitenstorfer, *Laser Photon. Rev.* **8**, 409 (2014).
- [S11] W. Sellmeier, *Ann. Phys. (Berlin)* **219**, 272 (1871).
- [S12] D. T. F. Marple, *J. Appl. Phys.* **35**, 539 (1964).
- [S13] A. Leitenstorfer *et al.*, *Appl. Phys. Lett.* **74**, 1516 (1999).